Desalination and Water Treatment
www.deswater.com

doi: 10.1080/19443994.2014.998715

57 (2016) 5183–5192
March

Taylor & Francis
Taylor & Francis Group

Thermal/plasma treatment effect on photocatalytic degradation of aqueous solution of methylene blue using Au-doped Fe/TiO_2 photocatalyst

Asif Mahmood[a,*], Shahid Mahmood Ramay[b], Yousef S. Al-Zaghayer[a,c], Shahid Atiq[d], Shahid Hussain Ansari[e]

[a]*Department of Chemical Engineering, College of Engineering, King Saud University, Riyadh, Saudi Arabia, Tel. +966 11 46 79966; Fax: +996 11 46 78770; email: ahayat@ksu.edu.sa (A. Mahmood), Tel. +966 11 46 76855; email: yszs@ksu.edu.sa (Y.S. Al-Zaghayer)*
[b]*Department of Physics and Astronomy, Colleges of Science, King Saud University, Riyadh, Saudi Arabia, Tel. +966 11 4678760; email: smramay@yahoo.com*
[c]*Supervisor of Industrial Catalysts Research Chair, King Saud University, Riyadh 11421, Saudi Arabia*
[d]*Centre of Excellence in Solid State Physics, University of the Punjab, New Campus, Lahore 54590, Pakistan, Tel. +92 300 7110532; email: shahidatiqpasrur@yahoo.com*
[e]*Centre for Energy Systems (CES), National University of Sciences and Technology (NUST), Islamabad, Pakistan, Tel. +92 51 9085 5116; email: shahid.ansari@ces.nust.edu.pk*

Received 13 August 2014; Accepted 9 December 2014

ABSTRACT

The effect of thermal/plasma treatment on the photocatalytic degradation of methylene blue (MB) using Au-doped Fe/TiO_2 photocatalyst was investigated. Iron (Fe)-doped TiO_2 samples were prepared by solgel auto-combustion technique. Later, gold nano-particles (AuNPs) were deposited on the as-prepared support (Fe/TiO_2) using conventional deposition–precipitation method with NaOH (DP NaOH), and the resulting catalysts were subsequently modified with thermal (at 450˚C under vacuum) and plasma (at an ambient temperature under Argon atmosphere for 20 min) treatments. To evaluate particle structure, size distribution, and composition, diverse analytical techniques such as X-ray diffractometer, BET surface area, SEM, EDX, and TEM were used. The photocatalytic activity was evaluated by assessing the degradation of the MB in water under ultraviolet (UV) irradiations while the parameters affecting photocatalytic process such as the catalyst crystallinity, light absorption efficiency, the dosage of catalyst, dopant, and MB concentrations were well controlled. Thermal-/plasma-treated samples showed significant enhancement in the photocatalytic activity compared to untreated samples by changing the morphology, increasing the number of AuNPs, improving the Au-doped Fe/TiO_2 interface, and decreasing the band-gap energies thus tuned Au-doped Fe/TiO_2 catalyst to higher efficiency. The AuNPs deposited on the Fe/TiO_2 showed good thermal stability as well. Based on the obtained results, it can be expected that the modified catalyst may have potential applications in various advanced technologies such as water treatment, sustainable energy, clean environment, and several others.

Keywords: Thermal/plasma; Photocatalytic degradation; Au nanoparticles; Fe/TiO_2; Methylene blue

---

*Corresponding author.

1. Introduction

The rising dependence on technology of our living standard requires more prospective applications in advanced technologies such as solar cells, water decontamination, purification and disinfection, air purification, and hydrogen production (solar light-induced water splitting), a rigorous research is needed to develop novel and the most effective photocatalysts materials compare to those available today [1–6]. TiO_2 is one of the potential photocatalysts that has been extensively studied and used as photocatalyst for the degradation of large number of organic and inorganic pollutants. Apart from photocatalytic behavior of TiO_2, it has various advantages such as its non-toxicity, relatively economical, chemical stability, anti-corrosive characteristics, and favorable opto-electronic properties. However, it has few limitations such as it works only under ultraviolet (UV) light because of its wide band gap (3.2 eV) and it has low photocatalytic activity because the occurrence of charge carrier recombination takes place within a very short time (nanoseconds) [7]. In order to enhance the performance of TiO_2 and overcome its limitations as a photocatalyst, more attention has been paid by incorporating transition metal ions to lower the band gap [7–9].

Many research groups [10–12] reported the doping effects of transition metal ions on the properties of TiO_2. Since the photocatalytic activity of the doped TiO_2 photocatalyst depends on various experimental conditions, preparation methods, nature, and concentration of the dopants ion, it is very hard to compare the results reported for doped samples. Among various dopants, the most favored dopants are iron (Fe) and gold (Au), as they have similar size to TiO_2. Recently, it is reported that catalytic activity of Fe/TiO_2 catalyst extensively improved as compared to Au/TiO_2 [13]. It is comprehensively reported that, the catalytic activity boosts as the mean particle size of Au decreases, and the optimum particle size is in between 2 and 4 nm [14–16].

In the present work, gold nano-particles (AuNPs) were deposited on the as-prepared support (Fe/TiO_2) and the resulting catalysts were subsequently modified with the thermal and plasma treatments. Thermal/plasma treatment has a momentous effect on the Au particle size and due to this reason, the specific surface area of the resulting catalysts decreased. Structurally, the thermal/plasma treatments reduced the size and increased the population of the AuNPs, improved the Au, Fe/TiO_2 interface, altered the textural properties and functionally, reduced the band gaps, and these traits contributed in improving the efficiency of the modified catalysts. In this article, we report on Au-doped Fe/TiO_2 photocatalysts modification by thermal and plasma treatment, as well as their photocatalytic activity in the aqueous solution of methylene blue (MB) using UV.

2. Experimental section

2.1. Synthesis techniques

To prepare Fe-doped TiO_2 particles, commercially available tetra-*n*-butyl titanate (Ti $(OC_4H_9)_4$, Wylson-Chem Co. Ltd, CAS No.: 5593-70-4) and iron nitrate (Fe $(NO_3)_3.9H_2O$, 99.99% pure, Sigma–Aldrich) were used as the starting materials in the proper stoichiometric ratios for solgel auto-combustion method, while the glycine (NH_2CH_2COOH, 99% pure, Sigma–Aldrich) was used as a fuel agent. The metal nitrate to glycine ratio was adjusted to 1:2. During synthesis, precisely calculated amounts of the starting materials were first dissolved in 50 mL of deionized water and later dried at 100℃ under continuous stirring for about one hour. In this way, a brownish color xerogel was obtained through stirring and heating at 150℃ on a hot plate. The dried powder was then heated at 400℃ for 2 h in a muffle furnace in air.

Secondly, in order to enhance the photocatalytic activity of TiO_2 to the maximum limit, we deposited 5 wt. % Au (AuCl, Acros) onto Fe-TiO_2 using the deposition–precipitation method. The detailed conventional deposition–precipitation method with NaOH (DP NaOH) and conditions of thermal/plasma treatment were described somewhere [16].

2.2. Catalysts characterization

Structural characterizations of all the Au-doped Fe/TiO_2 photocatalysts were performed using X-ray diffractometer (XRD) (Brucker, D8 diffractometer) using Cu Ke Au-doped Ti ($\lambda = 1.5406$ D8 diffractometer) using Cu Ke Au-dope. The morphology of the as synthesized (Pristine sample) and modified (thermal and plasma treated) photocatalysts was examined by scanning electron microscopy (SEM), JEOL JSM-7600F, FESM, Japan, and elemental analysis was carried out by attached EDS analysis (Oxford instruments, UK). Transmission electron microscopy (TEM) studies were done using JEOL 2100F, FEG-TEM, Japan. The specific surface area, pore volume, and average pore diameter of the catalysts were measured using Micromeritics Tristar ASAP 2020 surface area and porosity analyzer by N_2 adsorption data at 77 K according to the standard Brunauer Emmett Teller (BET) procedure. For each analysis, 0.25 g of catalyst was used. Prior to analysis, the degassing of the samples was done at 200˚C for 2 h to remove the moistness and weakly adsorbed gases from the catalyst surface. The absorbance spectra were recorded on UV absorbance spectra Labomed-2950, USA. UV–vis diffuse reflectance spectroscopy measurements were carried out to calculate the energy band gaps (E_g) of the synthesized composites using PerkinElmer's LAMBDA 35 UV–vis systems with integrating sphere accessory. The catalysts were further characterized by inductively coupled plasma atomic emission spectroscopy (ICP-AES) measurements.

2.3. Photocatalytic activity measurements

In this study, MB was exploited as pollutant molecule. The photocatalytic degradation of MB was carried out in a rectangular quartz reactor (30 mm × 40 mm × 60 mm). An MB aqueous solution (1.16×10^{-5} M) was photocatalyzed in a quartz reactor at room temperature (25˚C under UV light irradiation). In order to maintain the temperature of MB solution in the photo-reactor, cold water was circulated around the solution. A high-pressure mercury lamp (450 W, principal wavelength 365 nm, and luminous intensity 0.4 mW/cm^2) served as the UV light source. 100 mg catalyst powders were dispersed into 100 mL MB aqueous solution (10 mg/l). Prior to irradiation; the suspension was sonicated in the dark to disperse the catalyst in dye solution and certain attention was given to the continuous stirring of the solution during the whole experiment. After irradiation at a given reaction time (0 to 390 min by an increment of 30 min), about 2 mL of the mixed suspensions was extracted and filtered to separate the catalyst from the dye solution then the absorbance and degradation rates were determined by a UV a filtered to separate. The scanning wavelength range was from 300 to 750 nm. In this study, all the experimental and characterization conditions/tools are similar as in the previous research works [17] except the addition of Fe.

3. Results and discussion

3.1. Structural analysis

Fig. 1 shows XRD patterns of all catalysts and the peaks position are well agreed with the reflection of TiO_2 anatase crystal structure (JCPS card No. 00-021-1272). The distinctive peaks at $2\theta = 25.3^\circ$, 37.8˚, 47.7˚, 54.0˚, 62.4˚, and 76.02˚ corresponding to the anatase crystal planes are observed in all samples. Fe peaks could not be identified in Fig. 1. Since the ionic radius of Fe^{3+} (0.64 A˚) was slightly smaller than that of Ti^{4+} (0.68A˚) [18], so it can be supposed that all of the iron ions were incorporated into the structures of titania and replaced the titanium ion or located at the interstitial site. XRD peaks of metallic gold were observed (JCPS card No. 00-004-0784) in Fig. 1(b)–(e). The distinctive peaks at $2\theta = 44.39^\circ$, 64.57˚, and 77.54˚ corresponding to the metallic gold were observed in all the samples Fig. 1(b)–(e). Even after thermal/plasma treatment, no change in the crystal structure was observed as shown in XRD patterns (Fig. 1(b)–(e)).

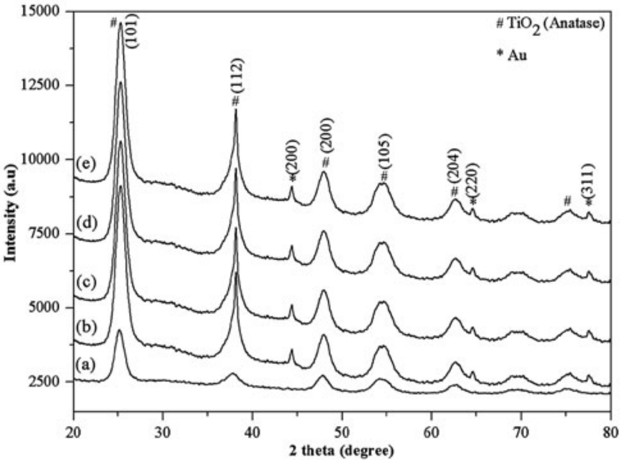

Fig. 1. XRD patterns of catalysts (a) Fe/TiO_2, (b) Au-doped Fe/TiO_2, (c) thermal, (d) plasma, and (e) thermal/plasma treated.

Particle morphology of as synthesized Au-doped Fe/TiO_2 catalyst sample is evident from the SEM images shown in Fig. 2. It can be observed from Fig. 2 that thermal/plasma treatment leads to a smaller TiO_2 particle. Based on these SEM images, it may be postulated that the thermal-/plasma-treated samples might have enhanced photocatalytic activity owning small particle size of TiO_2. Furthermore, characteristic peaks recorded in the EDX spectra elucidate the presence of Au and other elemental constituents of the catalysts such as Fe, Ti, and O as shown in insets of Fig. 2(a)–(c).

TEM studies are very helpful in understanding the exact morphology, structure, dimensions, and distribution of Au nanoparticles on TiO_2 support, as shown in Fig. 3. Although the same amount of Au nanoparticles (AuNPs) was deposited during the catalysts preparation but thermal modification followed by plasma treatment substantially affected the size and population of the Au nanoparticles on the surfaces of TiO_2 support than untreated samples, as displayed in Fig. 3(b) and AuNPs separately dispersed in solution.

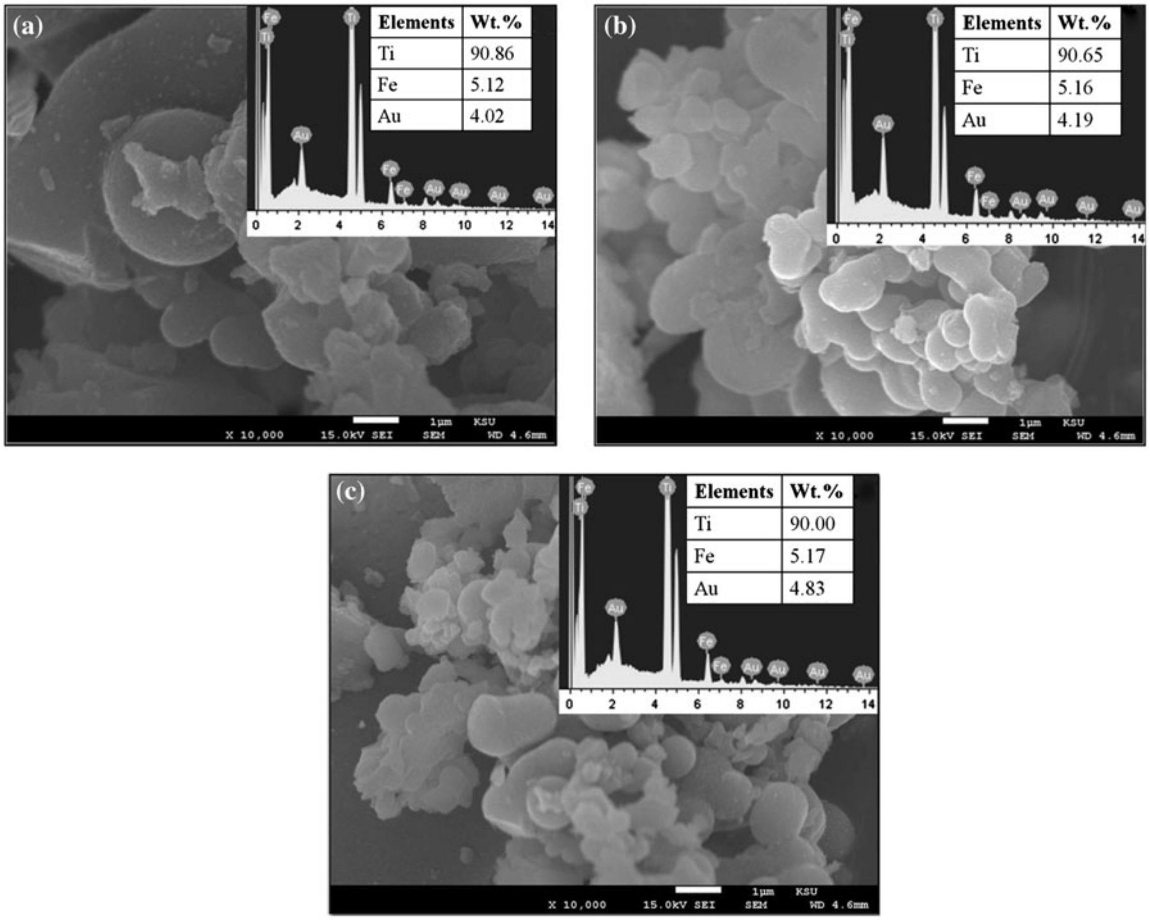

(a)

Elements	Wt.%
Ti	90.86
Fe	5.12
Au	4.02

(b)

Elements	Wt.%
Ti	90.65
Fe	5.16
Au	4.19

(c)

Elements	Wt.%
Ti	90.00
Fe	5.17
Au	4.83

Fig. 2. SEM micrographs of (a) Au-doped Fe/TiO_2, (b) thermal, and (c) thermal/plasma treated.

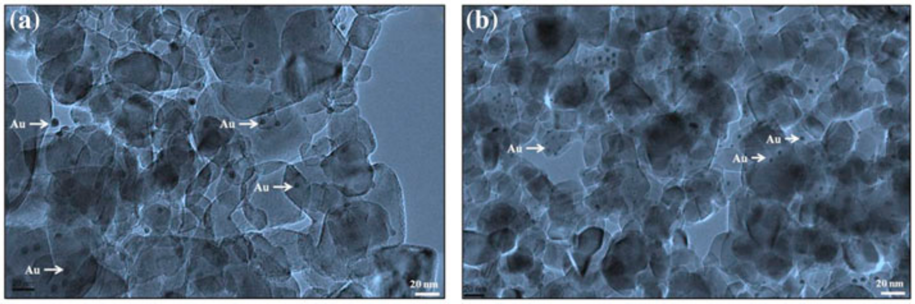

Fig. 3. TEM images of Au-doped Fe/TiO_2 catalysts samples (a) Au-doped Fe/TiO_2-indicating the attachment of Au nanoparticles (white arrows) on TiO_2 support and (b) thermal-/plasma-treated samples exhibiting fine Au nanoparticles at TiO_2 surfaces.

Quantitative analysis further confirmed the size refinement of the Au nanoparticles for modified catalyst (2–3 nm), shown in Fig. 3(b), compared to untreated samples which showed diameters in the range of 4~5 nm (Fig. 3(a)). This diametric reduction of Au nanoparticles may be attributed with the plasma sputter processing, (i) it is quite possible that the Au nanoparticles undergone sever mechanical loading upon plasma ions bombing resulting in the compaction of Au nanoparticles into smaller size and (ii) the other possibility is the disintegration of the Au nanoparticles under severe plasma sputtering conditions which probably turned nanoparticles to smaller dimensions [19].

Furthermore, high resolution transmission electron microscopy (HR-TEM) studies further confirm the size confinement of the Au nanoparticles after thermal/plasma treatment, as exhibited in lattice resolved images of the Au-doped TiO_2 catalyst (see Fig. 4).

HR-TEM images recorded on individual Au-doped Fe/TiO_2 catalyst constituent provide further insight into the structure and the catalyst constituents. Lattice resolved TEM images, Fig. 4, shows Au nanoparticles composed of a single-crystal metal having (1 1 1) planes and having a sharp interface with the (0 0 4) crystal planes of TiO_2 anatase phase. The HR-TEM micrograph (Fig. 4) showed that the average interplanar distance of fringes was $(0.67 + 0.73 + 0.89/3) - 0.76$ nm, which was in good agreement with the (1 1 1) plane of Au.

The results obtained from ICP-AES (OPTIMA 4300 DV (Perkin-Elmer, USA), Power: 1,300 W, Amount of catalyst = 0.25 g) confirmed that the Au particles increased for plasma treated and thermal-/plasma-treated samples as compared to untreated (As received sample) and thermal-treated samples (see Table 1). This implies that plasma and thermal treatments lead to a greater number of Au particles deposited on the TiO_2 surface.

Specific surface area (BET), pore volume (PV), and average pore size (PD) of the Au-doped Fe/TiO_2 and thermal- and plasma-treated catalysts are summarized in Table 2.

The PV and PD were calculated from adsorption branch of the respective N_2 adsorption–desorption isotherms (see Fig. 5) by applying Barrett, Joyner, and Halenda (BJH) method. According to the IUPAC classification both adsorption/desorption isotherms were of a mixed type (I/II form). Moreover, it is also apparent from Table 2 that Au nanoparticles size confinement has a notable effect on textural properties, especially on pore volume of the prepared catalysts. Au-doped Fe/TiO_2 sample showed relatively higher specific surface area and pore volume than that of thermal-/plasma-treated sample. For instant, the BET surface area and pore volume of Au-doped Fe/TiO_2 sample were 53.10 m^2/g and 0.47 cm^3/g, while for thermal-/plasma-treated Au-doped Fe/TiO_2 both were 45.67 m^2/g and 0.32 cm^3/g, respectively, which was in good agreement with the results determined by SEM and TEM.

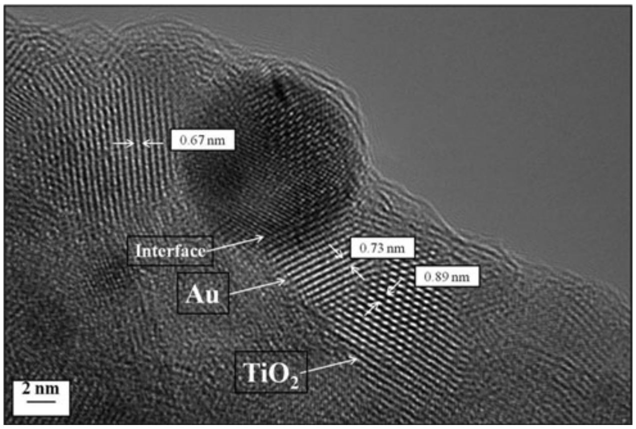

Fig. 4. HR-TEM images of modified catalyst, Au nanoparticles (white arrow) attached with TiO_2 surface and Lattice resolved HR-TEM image of the Au nanoparticle and TiO_2 crystal-interface is very clear.

Table 1
ICP-AES results of Fe/TiO_2, Au-doped Fe/TiO_2, thermal, plasma, and thermal/plasma treated

Compositions	Au (wt. %)
Au-doped Fe/TiO_2	4.38
Thermal-treated Au-doped Fe/TiO_2	4.47
Plasma-treated Au-doped Fe/TiO_2	4.86
Thermal-/plasma-treated Au-doped Fe/TiO_2	4.89

In comparison with Au-doped Fe/TiO_2 sample, the smaller pore volume in case of thermal- and plasma-treated sample is probably resulted due to partial blockage of the pores with active metal particles. Similar kinds of alterations in textural properties due to partial blockage of pores with active metal particles were also reported by various researchers in the literature [20].

3.2. Photocatalytic performance

The effect of thermal and plasma treatment on the photocatalytic activity was evaluated by estimating the band gap and the photo-absorption spectra technique. The energy band gap (Eg) of Au-doped Fe/TiO_2 and thermal-/plasma-treated samples can be calculated using Eq. (1) [21].

$$\alpha hv = A(hv - Eg)^{n/2} \quad (1)$$

where α, v, Eg, and A are absorption coefficient, light frequency, band-gap energy, and a constant, respectively, and n based on the nature of optical transition of a semiconductor for example $n = 1$ stands for direct transition whereas $n = 4$ stands for indirect transition. For TiO_2 $n = 1/2$, which corresponds to an indirect transition. The calculated band-gap energy of

Table 2
Textural properties and band-gap energies of Au-doped Fe/TiO_2 supported catalyst

Samples	Surface area (m^2/g)	Pore volume (cm^3/g)	Average pore size (nm)	Band-gap energy (eV)
Au-doped Fe/TiO_2	53.10	0.47	38.27	2.79
Thermal-/plasma-treated Au-doped Fe/TiO_2	45.67	0.32	31.67	2.65

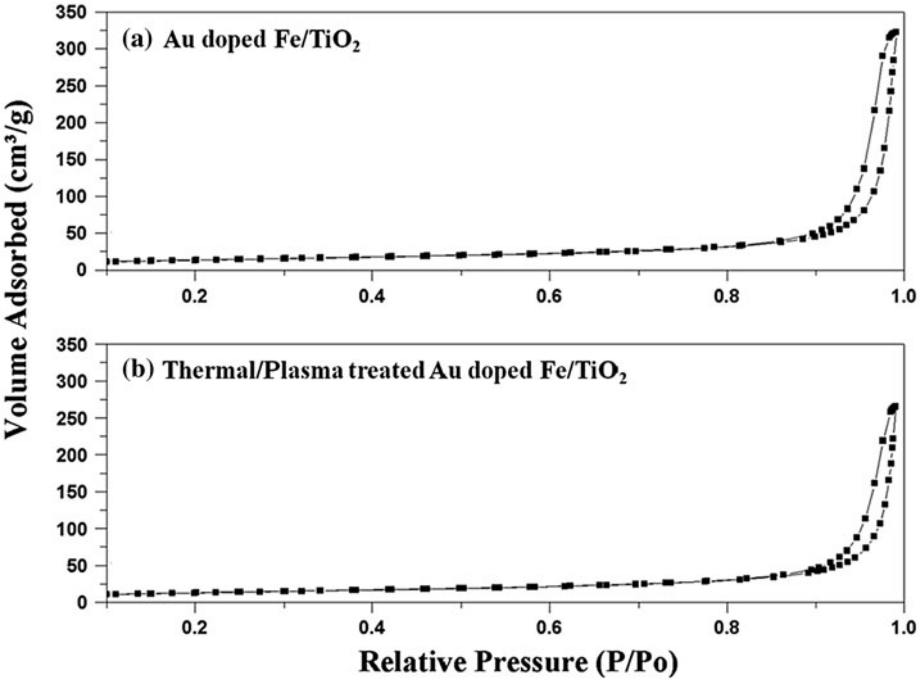

Fig. 5. N2 adsorption–desorption isotherms for (a) Au-doped Fe/TiO_2 and (b) thermal-/plasma-treated Au-doped Fe/TiO_2.

Au-doped Fe/TiO_2 sample and thermal-/plasma-treated Au-doped Fe/TiO_2 have decreased to 2.79 and 2.65 eV, respectively, (as shown in Table 2) in comparison with pure TiO_2 (P25) which is around 3.0–3.2 eV [22]. The surface modification with Au particles can cause a redshift of around 0.14 eV. The decrease in band-gap energy of Au-doped Fe/TiO_2 nano-composites may be due to the band shrinkage effect which is resulted from the AuNPs deposition on TiO_2 surface [23].

The sharp tangents (see Fig. 6) were drawn to examine the band gaps of the fabricated catalyst and obtained reduced band gaps 2.79, 2.75, 2.68, and 2.65 eV for the Au-doped Fe/TiO_2, thermal, plasma, and combined thermal-/plasma-treated samples, respectively.

Fig. 7 shows the photo-absorption spectra of the degraded dye solutions with respect to light-exposure durations ranging from 0 to 390 min. It is clearly evident that the absorption of MB gradually decreased with increasing irradiation time; however, different values of the degree of reduction were observed for each catalyst. The least degradation was observed after illuminating the solution for 390 min under UV–vis light that can be seen in Fig. 7(a). For the thermal-/plasma-treated Au-doped Fe/TiO_2 catalyst in the same sample, the MB showed a promising degradation even after 180 min exposure to UV–vis light, as displayed in Fig. 7(d). It can be seen that the maximum absorbance at 665 nm rapidly decreases with the increase in irradiation time and disappears almost completely after 210 min. The lack of any new-appearing peak in the course of the reaction showed that degradation had been successfully completed. These results confirm the enhanced photocatalytic activity of the modified samples in the UV light compared to untreated samples.

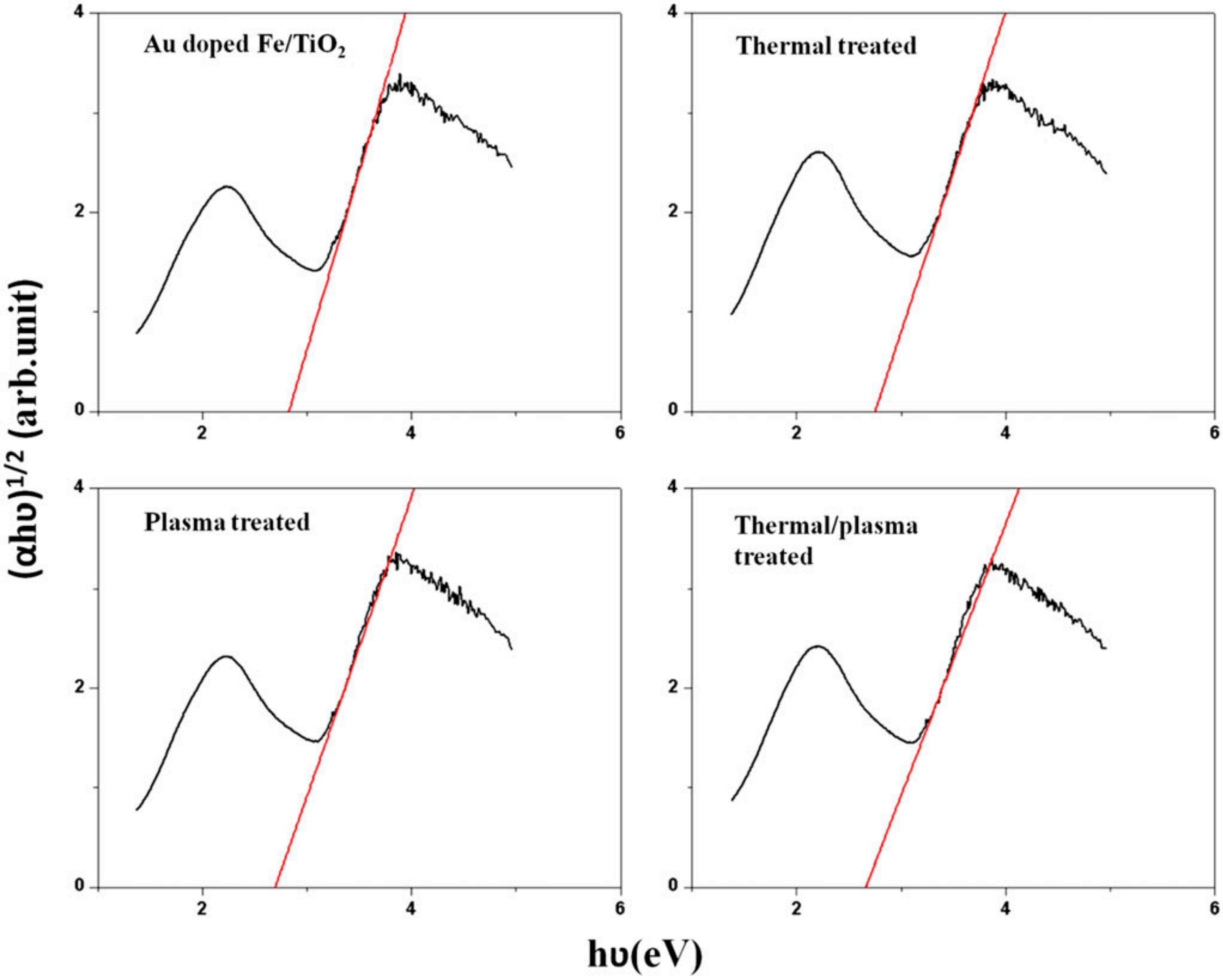

Fig. 6. $(\alpha h\nu)1/2$ vs. photon energy ($h\nu$) of Au-doped Fe/TiO$_2$, thermal, plasma, and thermal/plasma treated.

Such enhanced photocatalytic performance can be attributed to the excellent electronic conductivity and enhanced mass transportation, which facilitates photo-induced electron transport to the surface of the catalysts, thereby inhibiting recombination of photo-induced electrons and holes [24].

Although the same amounts of Au nanoparticles were introduced during the catalysts synthesis but our TEM and ICP-AES analysis showed significant changes in the diameters and population of Au nanoparticles after thermal followed by plasma treatments. Since the Au nanoparticles expedite the transport of photo-generated electrons and facilitate the longer charge separation by trapping them which in result displayed positive effect on the MB degradation [16].

Plasma sputtering improved the uniform distribution of the catalytic active species in the catalyst by converting the large Au nanoparticles into relatively smaller nanoparticles and our results are well agreed with the reported cases [16,25]. Thus, it can be postulated that the size confinement of Au nanoparticles due to thermal/plasma process increase the number of photo-generated electrons and holes in order to contribute in the photocatalytic reaction which in result enhanced the photocatalytic activity [25]. Furthermore, our results also showed an interesting sequence related to the photocatalytic activity of the catalyst samples. The order for MB degradation of Au-doped Fe/TiO$_2$ catalysts was related to type of processing done on the catalysts, and the results showed MB degradation for thermal/plasma > plasma > thermal treatment > as received (Au-doped Fe/TiO$_2$) samples. This sequence degradation exactly follows the order of band gaps

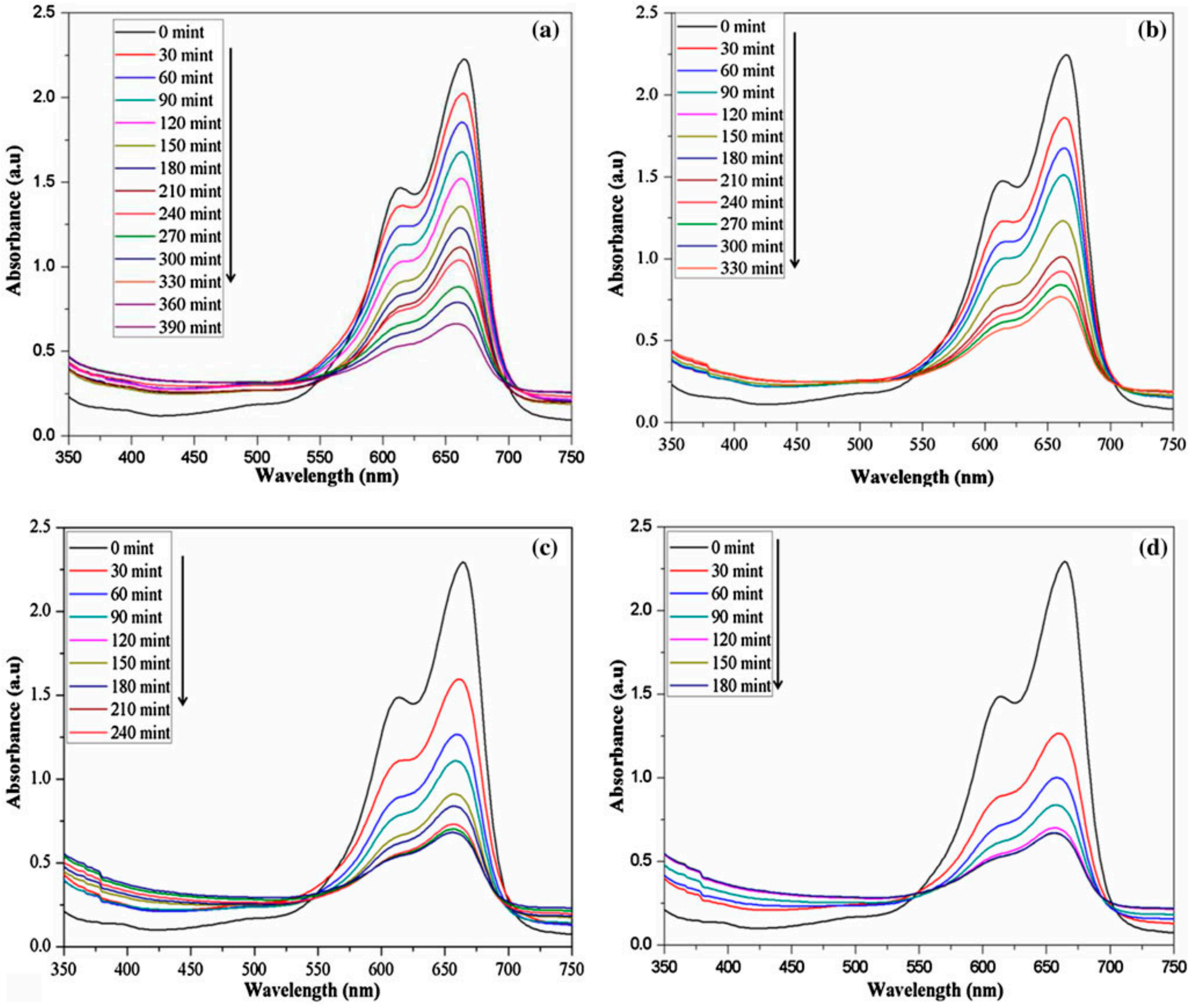

Fig. 7. Time-dependent UV–vis absorption spectra of (a) Au-doped Fe/TiO_2, (b) thermally treated Au-doped Fe/TiO_2, (c) plasma-treated Au-doped Fe/TiO_2, and (d) thermal-/plasma-treated Au-doped Fe/TiO_2.

obtained for all samples. The decreased band gap by the thermal and plasma treatment of Au-doped Fe/TiO_2 catalyst demonstrates the effectiveness of the synthesis catalysts for MB degradation in the UV–vis irradiation. Based upon these results, it may be elucidated the thermal/plasma treatment controlled the morphology and population of the Au nanoparticles. The size confinement of the Au nanoparticles decreased the band gap and the increased in numbers of active sites thus improved the quality of the Au-doped TiO_2 catalyst, which was confirmed experimentally by assessing the degradation of MB in the presence of modified catalyst.

The reaction mechanism for the degradation of MB over AuNPs-doped Fe/TiO_2 under UV irradiation has been explained in detail. After UV irradiation, the electrons available in the valance band get activation to the conduction band since the band gap of TiO_2 lies in the UV region [26]. In the conduction band, on the surface of support, electrons might be further shifted to the adsorbed O_2 to form the superoxide radical anions. Apart from this, in the case of AuNPs-doped Fe/TiO_2, the AuNPs can be considered as an electron sink, where the electrons in the conduction band can migrate to the noble metal surface, thereby preventing the recombination of electron hole pairs [26]. As a result, the shifting of electrons from the inside of the samples to the surface results in enhancement of photocatalytic efficiency that might be the reason for the improved photo catalytic activity for the existed AuNPs-doped samples under UV irradiation.

Fig. 8 shows time-dependent degradation of all the samples. It is clearly evident that the absorption of MB gradually decreased with increasing irradiation time; however, different values of the degree of reduction were observed for each catalyst.

Fig. 9 also shows that the performance of all samples. % degradation was calculated using Eq. 2.

$$\% \text{ degradation} = (1 - C/C_o) \times 100 \tag{2}$$

C_o is the initial concentration, C is the concentration after adsorption at different time. Thermal-/plasma-treated Au-doped Fe/TiO_2 showed higher degradation (70%) compare to other samples.

4. Conclusions

The effect of thermal/plasma treatment on the photocatalytic degradation of MB using Au-doped Fe/TiO_2 photocatalyst was investigated. The photocatalytic activity was gauged by assessing the degradation of MB in the presence of catalysis under UV light spectra. Our results showed that the quality of Au-doped Fe/TiO_2 catalyst was significantly improved by the thermal/plasma treatments. After the thermal and plasma treatment, the specific surface area of the Au-doped Fe/TiO_2 samples decreased. Due to the thermal/plasma treatments, the size of AuNPs reduced that increase the population of the Au nanoparticles. Thermal/plasma treatment improves the Au/TiO_2 interface, altered the textural properties and functionally, reduced the band gaps and these traits contributed in improving the efficiency of the catalysts. Concisely, combined thermal/plasma treatment is an effective method to obtain Au-doped Fe/TiO_2 with better photocatalytic performance and the catalysts may have potential applications in waste water disinfection, energy harvesting, solar technology and air purification, and many others.

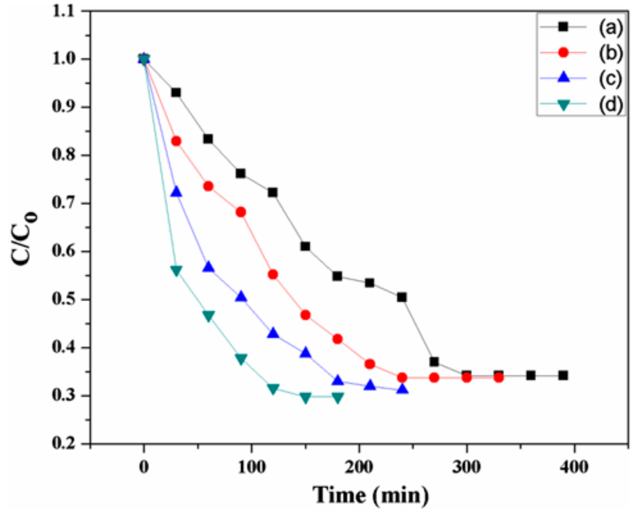

Fig. 8. Time-dependent degradation of (a) Au-doped Fe/TiO_2, (b) thermally treated Au-doped Fe/TiO_2, (c) plasma-treated Au-doped Fe/TiO_2, and (d) thermal-/plasma-treated Au-doped Fe/TiO_2.

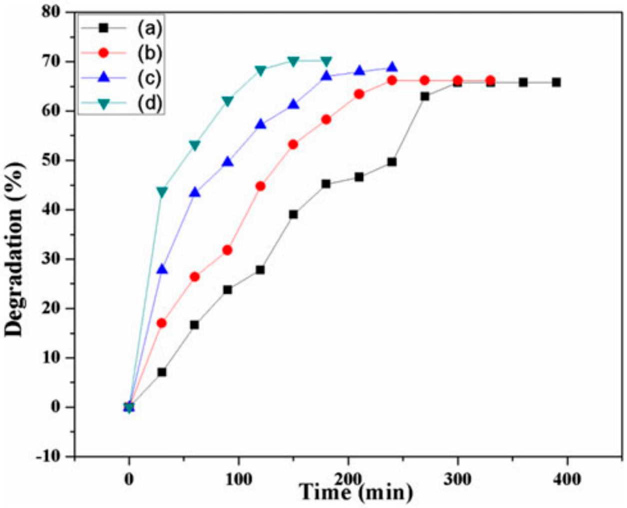

Fig. 9. % Age degradation of the dye pollutant using (a) Au-doped Fe/TiO_2, (b) thermally treated Au-doped Fe/TiO_2, (c) plasma-treated Au-doped Fe/TiO_2, and (d) thermal-/plasma-treated Au-doped Fe/TiO_2.

Acknowledgements

The Authors extend their appreciation to the Deanship of Scientific Research at King Saud University for funding the work through the research group project No. RGP-VPP-311.

References

[1] L.M. Pastrana-Martínez, J.L. Faria, J.M. Doña-Rodríguez, C. Fernández-Rodríguez, A.T.M. Silva, Degradation of diphenhydramine pharmaceutical in aqueous solutions by using two highly active TiO_2 photocatalysts: Operating parameters and photocatalytic mechanism, Appl. Catal. B 113–114 (2012) 221–227.

[2] L. Qi, J. Yu, M. Jaroniec, Preparation and enhanced visible-light photocatalytic H_2-production activity of CdS-sensitized Pt/TiO_2 nanosheets with exposed (001) facets, Phys. Chem. Chem. Phys. 13 (2011) 8915–8923.

[3] J. Du, X. Lai, N. Yang, J. Zhai, D. Kisailus, F. Su, D. Wang, L. Jiang, Hierarchically ordered macro-mesoporous TiO_2-graphene composite films: Improved mass transfer, reduced charge recombination, and their enhanced photocatalytic activities, ACS Nano 5 (2011) 590–596.

[4] R. Leary, A. Westwood, Carbonaceous nanomaterials for the enhancement of TiO_2 photocatalysis, Carbon 49 (2011) 741–772.

[5] C. Gomes Silva, R. Juárez, T. Marino, R. Molinari, H. García, Influence of excitation wavelength (UV or visible light) on the photocatalytic activity of titania containing gold nanoparticles for the generation of hydrogen or oxygen from water, J. Am. Chem. Soc. 133 (2011) 595–602.

[6] J. Zhang, Z. Xiong, X.S. Zhao, Graphene-metal-oxide composites for the degradation of dyes under visible light irradiation, J. Mater. Chem. 21 (2011) 3634–3640.

[7] A.T. Vu, Q.T. Nguyen, T.H.L. Bui, M.C. Tran, T.P. Dang, T.K. Tran, Synthesis and characterization of TiO_2 photocatalyst doped by transition metal ions (Fe^{3+}, Cr^{3+} and V^{5+}), Adv. Nat. Sci. Nanosci. Nanotechnol. 1 (2010) 015009–015013.

[8] M. Kitano, M. Matsuoka, M. Ueshima, M. Anpo, Recent development in titanium oxide-based photocatalysts, Appl. Catal. A: General 325 (2007) 1–4.

[9] D. Li, H. Haneda, Enhancement of photocatalytic activity of sprayed nitrogen-containing ZnO powders by coupling with metal oxides during the acetaldehyde decomposition, Chemosphere 54 (2004) 1099–1110.

[10] A. Davidson, M. Che, Temperature-induced diffusion of probe vanadium(IV) ions into the matrix of titanium dioxide as investigated by ESR techniques, J. Phys. Chem. 96 (1992) 9909–9915.

[11] M. Metikoš-Huković, M. Ceraj-Cerić, Investigations of chromium doped ceramic rutile electrodes, Mater. Res. Bull. 23 (1988) 1535–1544.

[12] T.M.D. Dang, T.M.H. Nguyen, H.P. Nguyen, The preparation of nano-gold catalyst supported on iron doped titanium oxide, Adv. Nat. Sci. Nanosci. Nanotechnol. 1 (2010) 025011–025018.

[13] S. Carrettin, Y. Hao, V.A. Guerrero, B.C. Gates, S. Trasobares, J.J. Calvino, A. Corma, Increasing the number of oxygen vacancies on TiO_2 by doping with iron increases the activity of supported gold for CO oxidation, Chem. Eur. J. 13 (2007) 7771–7779.

[14] M. Haruta, S. Tsubota, T. Kobayashi, M.J. Genet, B. Delmon, Low-temperature oxidation of CO over gold supported on TiO_2, O-Te_2O_3, and Co_3O_4, J. Catal. 144 (1993) 175–192.

[15] M. Valden, X. Lai, D.W. Goodman, Onset of catalytic activity of gold clusters on titania with the appearance of nonmetallic properties, Science 281 (1998) 1647–1650.

[16] A. Mahmood, S.I. Woo, Enhancement of catalytic activity of Au/TiO_2 by thermal and plasma treatment, Korean J. Chem. Eng. 30 (2013) 1876–1881.

[17] A. Mahmood, S.M. Ramay, Y.S. Al-Zaghayer, S. Atiq, I. Ahmad, M.A. Shar, S.D. Khan, Study the Structure and performance of thermal/plasma modified Au nanoparticle-doped TiO_2 photocatalyst, M. Phys. Lett. B 28 (2014) 1450208–1450220.

[18] P. Pongwan, B. Inceesungvorn, K. Wetchakun, S. Phanichphant, N. Wetchakun, Highly efficient visible-light-induced photocatalytic activity of Fe-doped TiO_2 nanoparticles, Eng. J. 16 (2012) 143–152.

[19] J. Wang, C. Liu, Y. Zhang, X. Zhu, F. He, Partial oxidation of methane to syngas over glow discharge plasma treated Ni-Fe/Al_2O_3 catalyst, Catal. Today 89 (2004) 183–191.

[20] J. Taghavimoghaddam, G.P. Knowles, A.L. Chaffee, Impact of preparation methods on SBA-15 supported low cobalt-content composites: Structure and catalytic activity, J. Mol. Catal. A: Chem. 377 (2013) 115–122.

[21] C. Liu, H. Lin, S. Gao, L. Guo, B. Huang, Y. Dai, AgI/AgCl/H_2WO_4 double heterojunctions composites: preparation and visible-light photocatalytic performance, Bull. Korean Chem. Soc. 35 (2014) 441–447.

[22] A.F. Shojaei, M.H. Loghmani, Effect of microwave irradiation on morphology and size of anatase nano powder: Efficient photodegradation of 4-nitrophenol by W-doped titania, Bull. Korean Chem. Soc. 33 (2012) 3981–3986.

[23] M.M. Khan, S.A. Ansari, J. Lee, M.H. Cho, Enhanced optical, visible light catalytic and electrochemical properties of Au/TiO_2 nanocomposites, J. Indus. Eng. Chem. 19 (2013) 1845–1850.

[24] Y.H. Kim, H.C. Choi, ZnO on thiolated graphene oxide as efficient photocatalyst for degradation of methylene blue, Bull. Korean Chem. Soc. 34 (2013) 3586–3590.

[25] B.Z. Tian, C.Z. Li, F. Gu, H.B. Jiang, Synergetic effects of nitrogen doping and Au loading on enhancing the visible-light photocatalytic activity of nano-TiO_2, Catal. Comm. 10 (2009) 925–929.

[26] M. Ghaffari, P.Y. Tan, M.E. Oruc, O.K. Tan, M.S. Tse, M. Shannon, Effect of ball milling on the characteristics of nano structure $SrFeO_3$ powder for photocatalytic degradation of methylene blue under visible light irradiation and its reaction kinetics, Catal. Today 161 (2011) 70–77.